$CaSiO_3$ crystals. Some spots show double the amount of carbon compared to the rest of the sample (*SI Appendix*, Fig. S3*F*). This could correspond to spots where decanol was highly integrated. On the surface of systems left reacting for 1 mo (CG and CGD), we notice larger-scale structures compared with 1 d of incubation. In the case of the CG system structures, crystals of $CaSiO_3$, NaCl, and $CaCO_3$ are visible. On the surface of the CGD systems, we observe $CaCO_3$, NaCl, and spots rich in Ca. Here again, we find spots with a high level of carbon that can be correlated to decanol integration (*SI Appendix*, Fig. S3 *K* and *M*). All the EDXS data confirmed the XPS previous conclusions. The increase of dimension of surface aggregates is directly related to the ongoing reaction time of the system. We can conclude from this analysis that decanol integration is increasing over time and is specific to CGD systems.

B.1. Decanol integration in chemical garden structures. As shown previously, when decanol is incubated with the sodium silicate system before calcium chloride addition, macroscopic-scale structures emerge that are different from typical chemical gardens. To understand whether decanol is integrated not only in the CGD samples surface, as implied by XPS and EDXS analysis, but also in the whole 3D CGD structures, we chose to perform a color-based assay. Decanol colored with Sudan Black B (2 mM) was layered on top of the silicate solution, and $CaCl_2$ powder was added to it. Systems were incubated for 1 d. The newly formed structures integrated Sudan Black B and remained stained with its color even after three washes (*SI Appendix*, Fig. S4) in their whole structure. As negative control, CG systems in the presence of SBB were created, and the SBB did not stain the CG crystals when no decanol was present. The integration of the dye as a proxy for the largely nonpolar decanol, even on a short time scale, supports the integration of the decanol in the crystal garden structures and supports the results from the EDXS analysis.

C. CGD Structure–Directed Membrane Assembly. Once decanol integration into the whole inorganic mineral structures was confirmed, we decided to test whether its presence could have supported fatty acid vesicle formation. We produced CG and CGD (1 mo) dried crystals, we cut small sections of them (~20 mg), trying to preserve their structure, placed them on the bottom of a cuvette, and added bicine buffer (0.2 M pH 8.5). We afterward pipetted decanoate, oleate, or myristoleate micelles to each cuvette in the following concentrations: 50 mM, 1 mM, and 5 mM, respectively. These concentrations are slightly higher (20%) than the critical vesicle concentration (CVC) reported in the literature (47) for each of the fatty acids used here. To check for vesicle formation, the absorbance at 400 nm was measured, and the resulting kinetics are shown in Fig. 3 *A*, *C*, and *D*. After the kinetics measure, CG and CGD crystals can still be visualized on the bottom of the cuvettes and their integrity seems to be conserved.

In the case of CGD systems, we observe absorbance variation with vesicle and micelle formation (see Fig. 3*A*, *SI Appendix*, Figs. S5 and S6). No absorbance variation or vesicles are instead noticed in the case of micelle addition to CG samples or to pure bicine buffer in this time frame. Decanoic acid shows an instantaneous increase of absorbance just after mixing with a stable high value; see Fig. 3*A*. This variation is related to supramolecular structure formation including membrane vesicles as confirmed with brightfield and fluorescence microscopy. Myristoleic and oleic acid show two different readouts, as can be seen in Fig. 3*A*, where the maximum level of absorbance is reached after a specific and different interval of time (1 min for myristoleic and 10 min for oleic acid). This is likely due to the different apparent pKa values for these fatty acids. We confirmed the presence of vesicles under these conditions using microscopy. The formation of vesicles under these conditions was further confirmed by a dye encapsulation test with 8-hydroxypyrene-1,3,6-trisulfonic acid (HPTS) addition to the bicine buffer. From the obtained images (Fig. 3*B* and *SI Appendix*, Figs. S5 and S6) we confirm vesicle formation for all three fatty acids. As an example, Fig. 3*B* shows clear encapsulation of HPTS inside membranes created using decanoic acid. We further analyzed vesicle formation using Merocyanine 540, a dye specifically sensitive to molecular packing. We observed that the incubation with CGD crystal lowers the critical vesicle concentration (CVC) of oleic, myristoleic, and decanoic acid. Data are shown in *SI Appendix*, Fig. S7. Furthermore, with respect to decanoic acid, CGD presence seems to shift the pH at which vesicles are formed, rendering feasible vesicle assembly at pH 8.5 (*SI Appendix*, Fig. S8). As a control, we studied vesicle formation and CVC with the buffer systems saturated with 1-decanol to determine whether the

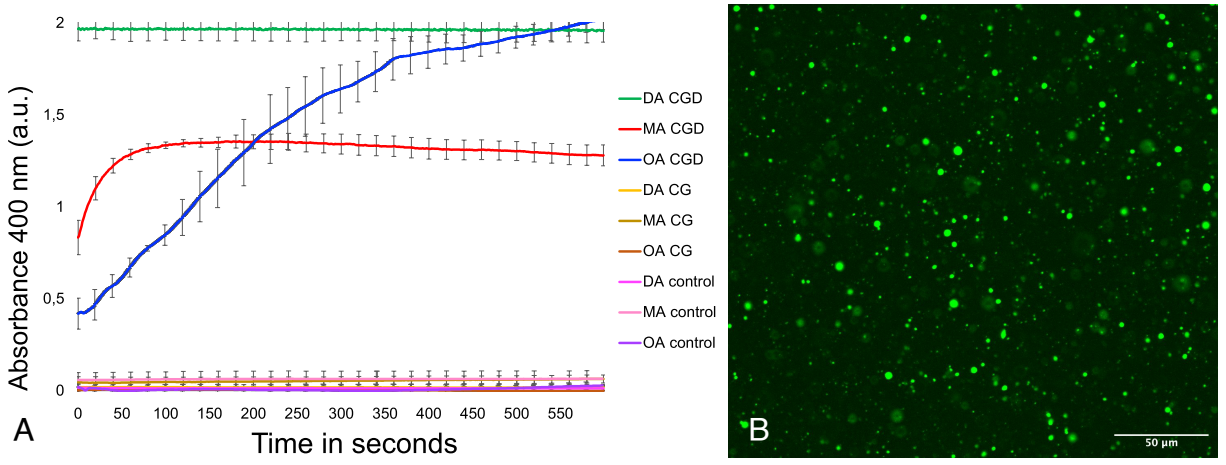

Fig. 3. CGD crystal-directed vesicle assembly. Vesicle formation was monitored in real time using changes in absorbance values. First, 0.2 M bicine buffer was incubated alone (control) or with CG or CGD samples. Fatty acids/soaps decanoate (DA), myristoleate (MA), or oleate (OA) were then added to the buffered solutions (*A*). Readings were performed in triplicate, normalized over the weight of crystals introduced in each cuvette and also through pure bicine buffer signal subtraction. Absorbance was registered each second for 10 min, and SE is reported for each 20-s interval. In *B*, fluorescence imaging of decanoic acid CGD-induced vesicle formation. Size bar 50 microns.

presence of a low soluble amount of decanol was responsible for the shift in CVC and vesicle formation. We determined that the presence of 1-decanol in solution was not sufficient to produce these results and that the presence of the CGD was necessary.

2. Conclusions

Many exploratory studies have shown that chemical gardens are a fertile and generative model system for prebiotic chemistry (48–51). They exhibit a broad range of nonlinear, pattern-forming chemical phenomena, the extent of which is still being discovered. While the relevance of hydrothermal vents and chemical gardens to the origins of life has long been recognized by the astrobiology community (3, 49, 52), the present work has taken steps by exploring how amphiphilic alcohols and acids—key components in protocell models—could have interacted with chemical gardens leading to the evolution of primitive cells.

We used silicate-based chemical gardens to implement an alkaline hydrothermal vent analogue. Integrating chemical gardens with a medium-chain alcohol, we generated a two-phase system where the alcohol was clearly separated from the silicate solution. The crystals localized at the interface showed random motion. Beneath the interface in the aqueous phase, new structures were created by the presence of decanol in the system. These new structures showed macroscopic and microscopic variability as well as compositional differences. As analyzed by XPS and EDXS, the materials comprising CG or CGD samples after 1 d or 1 mo of incubation appear similar in the overall atomic percentage. However, the observed structures are different. The integration of decanol on the inorganic surface changes the resulting morphology of the precipitates, and in the case of samples incubated with decanol, the decanol molecular interaction seems to increase salt aggregation upon the membrane surface, even if initially inhibiting the metal jets from the silicate surface. Furthermore, in the case of incubation with decanol, there are parts of the solid membranes which show an increased carbon presence. This likely correlates with decanol integration in the whole structure and that was confirmed through the Sudan Black B staining.

In conclusion, we demonstrated how medium-chain alcohols could have interacted with and evolved complex chemical garden structures. In a hydrothermal vent scenario, such structures could have aided the formation of supramolecular structures such as vesicles and micelles. These entities could have been composed of fatty acids exploiting fatty alcohol interaction. We in fact demonstrated that medium- (decanoic acid) and long-chain fatty acids (oleic and myristoleic), in the presence of chemical gardens formed in existence of decanol, are able to widely increase the creation of vesicles. These vesicles are generated even at concentrations close to the CVC, where their creation is normally minimal. We conclude that vesicles are formed and supported in our system only when the crystal garden is generated in the presence of decanol.

This work lays the foundation for the integration of organic compounds into silicate chemical gardens, including compounds that could have formed or helped vesicle formation such as fatty acids and fatty alcohols. Further studies could be performed on the interaction of other molecules such as DNA, amino acids, and enzymes inside hydrothermal vent–like structures and their compartmentalization into vesicles. This would lead to the creation of new experimental models that explore the interaction of inorganic and organic systems in the origin of life studies.

Materials and Methods

A. Materials. The following reagents were supplied by Merck Life Sciences: 1-decanol (150584), sodium silicate solution (338443), Sudan Black B and calcium chloride (anhydrous, granular, ≤7.0 mm, ≤93.0% C1016), decanoic acid (W236403), and myristoleic acid (M3325). Oleic acid was supplied from TCI Europe N.V. (112-80-1). Milli-Q water was obtained using PURELAB flex 2 ELGA LabWater. Tubes were provided by ROTILAB and 6-well plates from Corning Incorporated Costar. Cuvettes (01938-00) were provided from KARTELL SPA.

B. Vertical Observation System. Sodium silicate and Milli-Q water were mixed to obtain a 2.9 M solution at pH 11.5. This solution was placed inside glass vials of 12-mm diameter (Rotilab glass centrifuge tubes). Inside each glass vial were added in total 5 mL of solution: 5 mL of sodium silicate solution (Fig. 1*A*) or 4 mL of sodium silicate solution and 1 mL of 1-decanol (Fig. 1 *B* and *C*). Where the alcohol phase was introduced, 1 mL of 1-decanol was carefully layered on top of the silicate phase or mixed with it. Then, 300 mg calcium chloride seeds were dropped on the top of the solution manually. Systems were observed from the side and their evolution recorded over 2 h. The system was tested five times and repeatability confirmed. All the videos were recorded using C920 Logitech HD Pro.

C. Horizontal Observation System. First, 5 mL of 2.9 M Na_2SiO_3 solution was added to each well of a 6-well plate (Corning Incorporated Costar 6-well cell culture plate, flat bottom with a lid, tissue culture–treated nonpyrogenic polystyrene). In the experiments where fatty alcohol was introduced, 3 mL 1-decanol was carefully added on top of the aqueous phase (the minimum amount required to totally cover the sodium silicate phase). In the case of the 1-decanol integration control, decanol was colored through the addition of Sudan Black B (2 mM). Then, using a Carver hot press, 300 mg calcium chloride seeds were smashed, placed upon parafilm, and manually dropped in each well. Evolution of the system was recorded from above during the first 2 h, and images of the system were taken after 2 h. The system was tested five times and repeatability confirmed. In the case of samples left reacting 1 mo, the plate was sealed to avoid evaporation. As with the vertical observation system, all the videos were recorded using the C920 Logitech HD Pro webcam and all the Images taken using an iPhone 8 webcam and analyzed using Fiji. Images were inverted and pixel density maps created using Fiji's plot profile function. The mean pixels from an empty well were subtracted from the experimental values as background.

D. X-ray Photoelectron Spectroscopy. Sections of sodium silicate solution left reacting without (CG) and with decanol (CGD) were obtained from the surface of samples left reacting for 1 d in the horizontal system; the remaining liquid part was poured away and the solid one washed five times with Milli-Q water and pure ethanol and left to dry in a vacuum chamber for 1 wk. Parts of the obtained solids surfaces were cut and attached to a silicon wafer through carbon tape. CG and CGD samples were analyzed using and XPS apparatus located in an UHV (Ultra High Vacuum) analysis chamber equipped with a Mgk X-Ray source (photon at 1253.6 eV) and a hemispherical electron energy analyzer VSW (PSP power supply). The maximum energy resolution of the apparatus is 0.86 eV. Characterizations have been carried out at medium (PE = 50 eV) and high (PE = 20 eV) resolution. Single core levels were analyzed using Voigt functions for lineshape deconvolution after subtraction of a Shirley background.

E. SEM and SEM EDXS. Sections of sodium silicate solution reacted without (CG) and with decanol (CGD) were obtained from samples after 1 d or 1 mo in the horizontal system. The liquid part was poured away, and the solids were washed five times with Milli-Q water and left drying for 1 wk in a vacuum chamber. For each condition, three sections of the solid were cut and attached to a supporting stub and coated with Au or C depending on the type of analysis performed (SEM or EDXS respectively). A Jeol JSM-7001F SEM-FEG machine equipped with an Oxford INCA PentaFETx3 EDXS detector was used for morphological image acquisition and compositional analysis. SEM images were acquired using Secondary and Backscattering Electrons. SEM and EDXS analysis were performed at 15-keV beam energy and 10 mm of working distance.

F. Surface Directed Membrane Assembly. Oleic acid, decanoic acid, and myristoleic were added to a diluted NaOH solution to a final 250 mM concentration and mixed few minutes by vortex. Sodium bicine 0.2 M was produced dissolving bicine in Milli-Q water and adjusting the pH to 8.5 using NaOH 5 M. CG and CGD samples left reacting 1 mo were washed 5 times using Milli-Q and dried over 1 wk. Solids were afterward cut, leaving their surface as intact as possible and added to a plastic cuvette. Inside each cuvette, we tried to load a mineral crystal of ∼20 mg, and all the data are normalized over this standard weight. Fatty acids solutions were added to each cuvette to obtain a concentration of ∼20% higher than the CVC and mixed by pipetting. Final concentrations of decanoate, oleate, or myristoleate micelles were, respectively, 50 mM, 1 mM, and 5 mM. Kinetic measurements were run for 10 min, and absorbance value at 400 nm was recorded each second. Three replicates were analyzed, and data were normalized over the weight of crystals introduced on the bottom of the cuvette; background signal from pure bicine buffer with no fatty acid addition was subtracted. Vesicles formation was checked through the addition in each cuvette of HPTS (2 mM final concentration). After 10 min of incubation, the solutions were diluted 1:30 in dilution buffer (0.2 M bicine buffer pH 8.5, CVC of each corresponding acid, and 12% total volume of 1M glucose; this composition was specifically adapted to obtain a similar osmolarity in the dilution buffer to the buffer where the vesicles formed). Afterward, 70 μL of solution was charged in each well of 96-well Plate cell titer Ultra and visualized using the Nikon SIM with AX confocal microscope. The CVC was analyzed using merocyanine 540 (MC 540) addition in the presence of CG, CGD, and decanol. MC540 was dissolved in a 1:1 ethanol/water mix (1 mg/mL). Bicine buffer 0.2 M in Milli-Q was adjusted to pH 8.5 using NaOH. Phosphate buffer 0.1 M was prepared similarly. To 10 mL of buffer, 33 μL MC540 solution was added. Buffers were incubated with decanol, CG, and CGD, poured away after 10 min, and centrifuged at 13,000 rcf for 3 min. The obtained supernatants were used to run the CVC titrations. Absorbance values were obtained using the Spark Tecan plate reader and Corning transparent 96-well plates.

Data, Materials, and Software Availability. All study data are included in the article and/or *SI Appendix*.

ACKNOWLEDGMENTS. We would like to thank Michele Orlandi for the help on the analysis of Energy Dispersive X-ray Spectroscopy (EDXS) data, Nicola Bazzanella for the EDXS image acquisition, and Lucrezia Aversa and Roberto Verucchi for the X-ray Photoelectron Spectroscopy acquisition. We would also like to thank Giorgina Scarduelli for the help in imaging the fatty acid vesicles using the Nikon SIM AX, Graziano Guella for the help during revision, and Department of Cellular Computational and Integrative Biology High Throughput Screening facility for allowing us to use their Tecan plate reader. We would like to thank COST action Chemobrionics (CA17120) and DYNALIFE (CA21169) for giving us the opportunity to meet and conceive important ideas crucial for the manuscript preparation. We would also like to thank Department CIBIO Core Facilities which are supported by the European Regional Development Fund 2014 to 2020. This work was funded in part from the European Union's Horizon 2020 research and innovation programme under grant agreement No. 824060 (project ACDC).

Author affiliations: [a]Cellular, Computational and Integrative Biology Department, Laboratory for Artificial Biology, University of Trento, Povo 38123, Italy; [b]Division of Geological and Planetary Sciences, California Institute of Technology, Pasadena, CA 91125; [c]Instituto Andaluz de Ciencias de la Tierra, Consejo Superior de Investigaciones Cientificas–Universidad de Granada, Armilla, Granada 18100, Spain; [d]Instituto Carlos I de Física Teórica y Computacional, Universidad de Granada, Granada 18071, Spain; and [e]Chemical and Biological Engineering, University of New Mexico, Albuquerque, NM 87106

1. M. J. Russell, A. J. Hall, The emergence of life from iron monosulphide bubbles at a submarine hydrothermal redox and pH front. *J. Geol. Soc.* **154**, 377–402 (1997).
2. W. Martin, M. J. Russell, On the origin of biochemistry at an alkaline hydrothermal vent. *Philos. Trans. R. Soc. London Ser. B, Biol. Sci.* **362**, 1887–1925 (2007).
3. W. Martin, J. Baross, D. Kelley, M. J. Russell, Hydrothermal vents and the origin of life. *Nat. Rev. Microbiol.* **6**, 805–814 (2008).
4. J. H. Cartwright, M. J. Russell, The origin of life: The submarine alkaline vent theory at 30. *Interface Focus* **9**, 1–6 (2019).
5. S. F. Jordan *et al*., Promotion of protocell self-assembly from mixed amphiphiles at the origin of life. *Nat. Ecol. Evol.* **3**, 1705–1714 (2019).
6. G. Proskurowski *et al*., Abiogenic hydrocarbon production at lost city hydrothermal field. *Science (New York, N.Y.)* **319**, 604–607 (2008).
7. S. G. Sander, A. Koschinsky, Metal flux from hydrothermal vents increased by organic complexation. *Nat. Geosci.* **4**, 145–150 (2011).
8. M. Keith, F. Häckel, K. M. Haase, U. Schwarz-Schampera, R. Klemd, Trace element systematics of pyrite from submarine hydrothermal vents. *Ore Geol. Rev.* **72**, 728–745 (2016).
9. V. Sojo, B. Herschy, A. Whicher, E. Camprubí, N. Lane, The origin of life in alkaline hydrothermal vents. *Astrobiology* **16**, 181–197 (2016).
10. J. C. Walker, Carbon dioxide on the early earth. *Origins Life Evol. Biosphere* **16**, 117–127 (1985).
11. A. Ianeselli *et al*., Water cycles in a hadean CO_2 atmosphere drive the evolution of long DNA. *Nat. Phys.* **18**, 579–585 (2022).
12. T. Shibuya, K. Takai, Liquid and supercritical CO_2 as an organic solvent in hadean seafloor hydrothermal systems: Implications for prebiotic chemical evolution. *Progr. Earth Planet. Sci.* **9**, 1–15 (2022).
13. T. J. Wolery, N. H. Sleep, Hydrothermal circulation and geochemical flux at mid-ocean ridges. *J. Geol.* **84**, 249–275 (1976).
14. W. E. Seyfried, J. L. Bischoff, Experimental seawater-basalt interaction at 300°C, 500 bars, chemical exchange, secondary mineral formation and implications for the transport of heavy metals. *Geochim. Cosmochim. Acta* **45**, 135–147 (1981).
15. J. M. McDermott, S. P. Sylva, S. Ono, C. R. German, J. S. Seewald, Abiotic redox reactions in hydrothermal mixing zones: Decreased energy availability for the subsurface biosphere. *Proc. Natl. Acad. Sci. U.S.A.* **117**, 20453–20461 (2020).
16. D. A. Zaia, C. T. B. Zaia, H. D. Santana, Which amino acids should be used in prebiotic chemistry studies? *Origins Life Evol. Biospheres* **38**, 469–488 (2008).
17. R. Braakman, Mapping metabolism onto the prebiotic organic chemistry of hydrothermal vents. *Proc. Natl. Acad. Sci. U.S.A.* **110**, 13236–13237 (2013).
18. L. M. Barge, E. Flores, M. M. Baum, D. G. Velde, M. J. Russell, Redox and pH gradients drive amino acid synthesis in iron oxyhydroxide mineral systems. *Proc. Natl. Acad. Sci. U.S.A.* **116**, 4828–4833 (2019).
19. E. Branscomb, M. J. Russell, Frankenstein or a submarine alkaline vent: Who is responsible for abiogenesis? *BioEssays* **40**, 1700182 (2018).
20. M. J. Russell, Green rust: The simple organizing 'seed' of all life? *Life* **8**, 35 (2018).
21. Y. Novikov, S. D. Copley, Reactivity landscape of pyruvate under simulated hydrothermal vent conditions. *Proc. Natl. Acad. Sci. U.S.A.* **110**, 13283–13288 (2013).
22. M. Colin-Garcia *et al*., Hydrothermal vents and prebiotic chemistry: A review. *Bol. Soc. Geol. Mex.* **68**, 599–620 (2016).
23. A. Borrego-Sánchez, C. Gutiérrez-Ariza, C. I. Sainz-Díaz, J. H. E. Cartwright, The effect of the presence of amino acids on the precipitation of inorganic chemical-garden membranes: Biomineralization at the origin of life. *Langmuir* **38**, 10538–10547 (2022).
24. Y. Ding, J. H. Cartwright, S. S. Cardoso, Intrinsic concentration cycles and high ion fluxes in self-assembled precipitate membranes. *Interface Focus* **9**, 1–7 (2019).
25. S. Maurer, The impact of salts on single chain amphiphile membranes and implications for the location of the origin of life. *Life* **7**, 44 (2017).
26. S. F. Jordan, E. Nee, N. Lane, Isoprenoids enhance the stability of fatty acid membranes at the emergence of life potentially leading to an early lipid divide. *Interface Focus* **9**, 1–11 (2019).
27. P. Walde, R. Wick, M. Fresta, A. Mangone, P. L. Luisi, Autopoietic self-reproduction of fatty acid vesicles. *J. Am. Chem. Soc.* **116**, 11649–11654 (1994).
28. I. Budin, N. Prwyes, N. Zhang, J. W. Szostak, Chain-length heterogeneity allows for the assembly of fatty acid vesicles in dilute solutions. *Biophys. J.* **107**, 1582–1590 (2014).
29. M. M. Hanczyc, S. M. Fujikawa, J. W. Szostak, Experimental models of primitive cellular compartments: Encapsulation, growth, and division. *Science (New York, N.Y.)* **302**, 618–622 (2003).
30. M. M. Hanczyc, S. S. Mansy, J. W. Szostak, Mineral surface directed membrane assembly. *Origins Life Evol. Biospheres* **37**, 67–82 (2006).
31. K. Adamala, J. W. Szostak, Nonenzymatic template-directed RNA synthesis inside model protocells. *Science* **342**, 1098–1100 (2013).
32. A. N. Albertsen, C. D. Duffy, J. D. Sutherland, P. A. Monnard, Self-assembly of phosphate amphiphiles in mixtures of prebiotically plausible surfactants. *Astrobiology* **14**, 462–472 (2014), https://home.liebertpub.com/ast.
33. C. Bonfio, D. A. Russell, N. J. Green, A. Mariani, J. D. Sutherland, Activation chemistry drives the emergence of functionalised protocells. *Chem. Sci.* **11**, 10688–10697 (2020).
34. M. Fiore *et al*., Synthesis of phospholipids under plausible prebiotic conditions and analogies with phospholipid biochemistry for origin of life studies. *Astrobiology* **22**, 598–627 (2022).
35. C. L. Apel, D. W. Deamer, M. N. Mautner, Self-assembled vesicles of monocarboxylic acids and alcohols: Conditions for stability and for the encapsulation of biopolymers. *Biochim. Biophys. Acta (BBA) - Biomembr.* **1559**, 1–9 (2002).
36. P. A. Monnard, D. W. Deamer, Membrane self-assembly processes: Steps toward the first cellular life. *Anatom. Rec.* **268**, 196–207 (2002).
37. S. Kapoor *et al*., Prebiotic cell membranes that survive extreme environmental pressure conditions. *Angewan. Chemie* **126**, 8537–8541 (2014).
38. L. Misuraca *et al*., High-temperature behavior of early life membrane models. *Langmuir* **36**, 13516–13526 (2020).
39. L. Misuraca, B. Demé, P. Oger, J. Peters, Alkanes increase the stability of early life membrane models under extreme pressure and temperature conditions. *Commun. Chem.* **4**, 1–8 (2021).
40. T. M. Mccollom, G. Ritter, B. R. Simoneit, Lipid synthesis under hydrothermal conditions by Fischer-Tropsch-type reactions. *Origins Life Evol. Biosphere* **29**, 153–166 (1999).
41. P. A. Monnard, D. W. Deamer, Preparation of vesicles from nonphospholipid amphiphiles. *Methods Enzymol.* **372**, 133–151 (2003).
42. G. L. Früh-Green *et al*., 30,000 years of hydrothermal activity at the lost city vent field. *Science* **301**, 495–498 (2003).

43. K. A. Ludwig, D. S. Kelley, D. A. Butterfield, B. K. Nelson, G. Früh-Green, Formation and evolution of carbonate chimneys at the lost city hydrothermal field. *Geochim. Cosmochim. Acta* **70**, 3625–3645 (2006).
44. R. E. Mielke *et al*., Design, fabrication, and test of a hydrothermal reactor for origin-of-life experiments. *Astrobiology* **10**, 799–810 (2010).
45. A. F. M. Barton, Ed., *IUPAC Solubility Data Series. 15: Alcohols with Water* (Elsevier, 1984), vol. 15.
46. Y. Foucaud *et al*., Synergistic adsorptions of Na_2CO_3 and Na_2SiO_3 on calcium minerals revealed by spectroscopic and ab initio molecular dynamics studies. *Chem. Sci.* **10**, 9928–9940 (2019).
47. P. Walde, T. Namani, K. Morigaki, H. Hauser, *Formation and Properties of Fatty Acid Vesicles (Liposomes)* (Informa Healthcare, 2006), pp. 1–19.
48. L. M. Barge *et al*., Characterization of iron-phosphate-silicate chemical garden structures. *Langmuir* **28**, 3714–3721 (2012).
49. L. M. Barge *et al*., From chemical gardens to chemobrionics. *Chem. Rev.* **115**, 8652–8703 (2015).
50. S. S. Cardoso *et al*., Chemobrionics: From self-assembled material architectures to the origin of life. *Artif. Life* **26**, 315–326 (2020).
51. O. Steinbock, J. H. Cartwright, L. M. Barge, The fertile physics of chemical gardens. *Phys. Today* **69**, 44 (2016).
52. S. McMahon, Earth's earliest and deepest purported fossils may be iron-mineralized chemical gardens. *Proc. R. Soc. B: Biol. Sci.* **286**, 20192410 (2019).